nature photonics

Article

https://doi.org/10.1038/s41566-023-01188-y

Light sheets for continuous-depth holography and three-dimensional volumetric displays

Received: 19 December 2021

Accepted: 27 February 2023

Published online: 10 April 2023

Check for updates

Ahmed H. Dorrah[1], Priyanuj Bordoloi[1], Vinicius S. de Angelis[2], Jhonas O. de Sarro[2], Leonardo A. Ambrosio[2], Michel Zamboni-Rached[3] & Federico Capasso[1]

Projecting high-quality three-dimensional (3D) scenes via computer-generated holography is a sought-after goal for virtual and augmented reality, human–computer interaction and interactive learning. Three-dimensional objects are usually constructed from a single hologram by cascading a stack of two-dimensional (2D) scenes along the optical path and perpendicular to it. The spatial separation between those scenes, however, is fundamentally constrained by the numerical aperture of the hologram, limiting the axial resolution and depth perception of the generated 3D image. Here we propose a new class of hologram that instead projects a desired scene onto 2D sheets oriented perpendicular to the plane of the display screen, thus enabling continuous reconstruction of the object along the optical path. To achieve this, we decompose the target scene into threads of light—arrays of non-diffracting pencil-like beams whose envelopes can be locally structured along the propagation direction at will. Using a spatial light modulator, we project 2D scenes onto the plane normal to the hologram and by stacking multiple 2D sheets in parallel we construct 3D objects with high fidelity and low crosstalk. Computer-generated holography of this kind opens new routes to realistic 3D holography and can be deployed in wearable smart glasses, portable devices and wide-angle volumetric displays.

In contrast to photography, which stores a fixed view of a scene using a lens, a hologram records the entire wavefront scattered from an object, thus enabling more realistic reconstruction of the scene in terms of depth perception and parallax[1]. When suitably illuminated, holograms provide true-to-life playback of a three-dimensional (3D) target object that can be observed with the naked eye from different viewing angles. Although invented for the purpose of improving electron microscopy[2], holography has rapidly found application in volumetric displays[3], optical data storage[4,5], biological imaging[6,7], laser beam shaping[8], optical tweezers and micromanipulation[9] and virtual and augmented reality[10] due to the abundance of coherent sources and computer-generated holograms (CGHs). The latter are often recorded (in transmission or reflection) using liquid crystal displays[11,12], digital micromirror devices[13,14], erasable photorefractive polymers[15], stretchable materials[16] and metasurfaces[17,18], to name a few.

The quality of a holographic display relies on its ability to exhibit certain sources of information—often referred to as cues[19]—that collectively stimulate depth perception in the human visual system, allowing us to derive and understand the structure and depth of a natural complex scene. This includes relative object sizes, densities, heights and

[1]Harvard John A. Paulson School of Engineering and Applied Sciences, Harvard University, Cambridge, MA, USA. [2]Department of Electrical and Computer Engineering, São Carlos School of Engineering, University of São Paulo, São Paulo, Brazil. [3]School of Electrical and Computer Engineering, University of Campinas, São Paulo, Brazil. e-mail: dorrah@seas.harvard.edu; capasso@seas.harvard.edu

https://doi.org/10.1038/s41566-023-01188-y

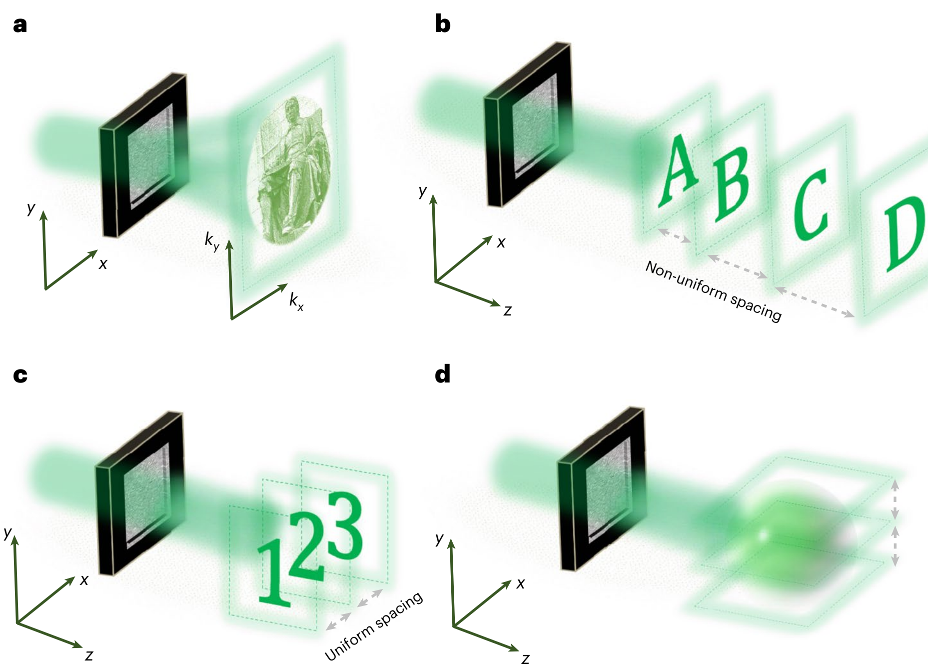

Fig. 1 | Different approaches to holographic projection. a, In Fourier holography, a 2D image is projected in the far field with limited depth of field. **b**, With multi-plane Fresnel holography, 2D images can be projected at different depths along the optical path, albeit with different sizes due to diffraction. To avoid crosstalk, images projected at farther distances must maintain larger separations between them, limiting the axial resolution and depth perception. **c**, Holographic light sheets are a new class of hologram that can project multiple images onto parallel layers oriented perpendicular to the hologram plane while preserving uniform separation between them. **d**, A 3D scene is decomposed into a stack of 2D holographic light sheets that can be oriented horizontally (as shown) or vertically, providing realistic reconstruction of the target object by projecting it with continuous depth along the axial direction.

aerial perspective, in addition to more subtle cues such as occlusion (hiding one object behind another), parallax (apparent displacement of an object depending on the observer's point of view), binocular disparity (changing relative position of an object as it is projected on each retina, separately) and convergence/accommodation (independent focusing on close/distant objects). Decades of effort has pushed the frontiers of holography in an attempt to achieve adequate compromises between these cues, ultimately producing photorealistic 3D images, aided by progress in wavefront-shaping tools and CGHs. Central to these advances is the ability to project a stack of images, with narrow gaps between them, to construct a true volumetric scene. Early pursuits of this goal started by assembling composite holographic stereograms in which a sequence of projections of 3D perspectives is first calculated with a Fourier-based transform, then grouped into a single CGH that reconstructs the target image, albeit in 2D, with a wide angle of view[20,21]. Iterative approaches using Fresnel holography—commonly known as the ping-pong algorithm—were later used to generate two noiseless image intensities at two depth locations from a single CGH by treating the phases relating the two images as a design degree of freedom[22]. Extensions of this method that project speckle-free images onto three planes have since been demonstrated[23]. Other approaches based on integral imaging[24] and dense ray sampling[25] reproduce an image with full parallax by deploying a two-dimensional (2D) array of microlenses that captures elemental images of the object as seen from the viewpoint of that lens's location. Horizontal/vertical parallax have also been achieved through stereograms[26–29], whereas true (3D) depth has been realized with multi-layered holography that now extends beyond several planes[30–37]. In parallel to these efforts, much progress has been made in developing holographic displays (recording media) themselves to refresh the projected holographic scene as a function of time; for example, by using updatable photorefractive polymers[3,38] or scannable photophoretic displays[39]. Other investigations studied spatiotemporal focusing using pulsed laser sources[40] or by enhancing the hologram resolution using nonlinear[41] and plasmonic metasurfaces[33,42], in addition to mitigating the trade-off between image size and viewing angle using speckle holography[43] and the synthetic aperture technique[44]. As this field matured, the search for fast hologram computation also began—a requirement that has been met by deploying look-up tables[45,46], accelerated GPUs[47] and, more recently, machine learning and deep neural networks[48,49].

Despite the advances in holography and its applications over the past few decades, there are still several limitations that prevent the projection of realistic 3D scenes like those depicted in science fiction movies. For example, Fourier holograms based on the well-known kinoform technique and its extensions[50,51] can primarily project objects within a short depth of focus at a far-field region (Fig. 1a), or in the vicinity of the focal plane of a lens, making them better suited for microscopy[52–54]—a limitation that has been addressed by Fresnel holography, which can project arbitrarily large images with 3D depth[55]. Fresnel holography, however, cannot maintain a uniform separation between the projected images without introducing crosstalk (Supplementary Note 1). This has been mitigated by preconditioning the wavefront such that it reduces to a Fourier hologram, locally, at the plane of interest while adding random phase values to render a quasi-orthogonal set of images with minimum interference[35]. The finite aperture size means that this approach (and Fresnel holography in general) still mandates progressively larger separations between the images projected at longer distance, as depicted in Fig. 1b, leading to non-uniform sampling of the 3D scene in the axial direction that in turn hinders many applications. The projection quality can be improved with cascaded diffractive elements[56] or cylindrical holograms[57], which often add complexity and cost. In short, a compact holographic mechanism that can enable accurate reconstruction of a 3D object using a single hologram, while achieving continuous depth with high axial resolution, remains elusive.

https://doi.org/10.1038/s41566-023-01188-y

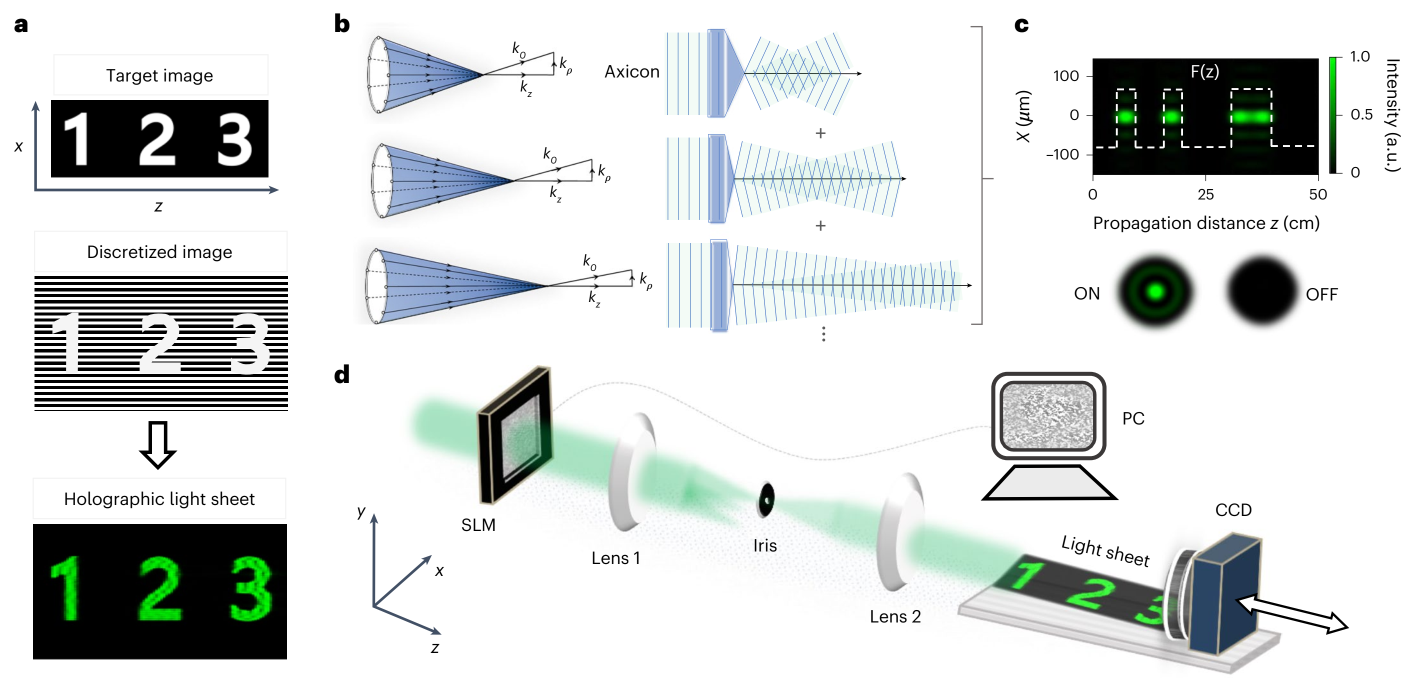

Fig. 2 | Concept of holographic light sheets. a, A target image is discretized, row by row, into a stack of parallel lines. These lines are then holographically reconstructed via threads of light in the x–z plane. **b**, Each forward-propagating light thread is created from a superposition of non-diffracting beams (Bessel modes), which can be generated by axicons with slightly different cone angles. Here, k_ρ and k_z denote the transverse and longitudinal wavenumbers of each Bessel beam, $k_0 = 2\pi/\lambda$. **c**, Top: a superposition of co-propagating Bessel beams with different cone angles (wavevectors) can be designed to spatially modulate its intensity profile along the z direction, following the target profile specified by $F(z)$. Bottom: transverse cross-sections of the beam at two different z planes exhibiting the intensity modulation in the beam's centre. **d**, Holographic light sheets are generated by encoding a phase-only CGH onto an SLM. A horizontally polarized light beam (532 nm) is expanded and collimated, approximating quasi-plane-wave illumination onto the SLM. The output beam from the SLM is imaged and filtered using a standard 4f lens system to get rid of higher diffraction orders and project the desired image onto a CCD. The CCD is mounted on a translational stage to record the generated pattern at each z plane. By stacking 1D slices (at the plane $y = 0$) from these images in the axial direction, the longitudinal profile of the hologram can be reconstructed in the x–z plane. a.u., arbitrary units.

In this work, we propose and experimentally demonstrate a new approach to holography that addresses the above constraints. In contrast to the wide body of literature that seeks to project one or more scenes onto the plane(s) parallel to the display, here we project each scene onto a flat light sheet, oriented perpendicular to the display as illustrated in Fig. 1c. This enables us to sample the target image continuously along the propagation direction with high axial resolution. We achieve this by decomposing any desired target image into threads of light whose intensities can be structured at will along the optical path. By assembling an array of those light threads, we synthesize 2D sheets that can then be closely stacked in parallel and with equal separation to construct the desired 3D scene with high fidelity, low crosstalk and long depth of field (Fig. 1d). Our approach provides means to achieve realistic 3D holography. It can also be integrated in volumetric displays by projecting the light sheets in lightly scattering media[58] or onto a stack of LCD panels[59], thus visualizing a volumetric object from virtually any angle. Furthermore, our formulation is based on a non-iterative closed-form analytic solution, providing calculable computation costs. We thus expect this technique to open new routes to real-time 3D holography, augmented and virtual reality and wide-angle volumetric displays.

Holographic light sheets

Concept

Our goal is to first create a thread of light that can be structured along the optical path, and then assemble several threads into 2D sheets that can be stacked to form the desired volumetric scene. Our light threads take the form of a superposition of non-diffracting beams with different tilt angles that constructively (destructively) interfere at precise locations along the axial direction to sculpt any predetermined intensity profile. By combining multiple threads in parallel, the target scene can be rastered, row by row, as is done in 3D printing. More specifically, each thread is composed of a discrete superposition of forward-propagating Bessel modes with different cone angles (propagation constants), weighted by carefully chosen complex coefficients (which vary in amplitude and phase), enabling full control over the intensity of the resulting envelope at each propagation distance. This approach, commonly referred to in the literature as frozen waves, is detailed more fully in ref. 60 and in the Methods. We choose Bessel beams because of their quasi diffractionless and self-healing properties, which allow the beam to reconstruct its central spot even if obstructed by an obstacle[61]. This serves our purpose for generating robust 3D holograms with long depth of field. By assembling many frozen waves into a 2D sheet, one can construct a surface with an arbitrary intensity profile oriented along the propagation direction with full control over the intensity at each point[62].

To illustrate this concept, first assume that we wish to project the target image shown in Fig. 2a onto the horizontal (x–z) plane. We start by discretizing this 2D image into parallel threads of light that travel along the z direction; the envelope of each light thread is designed to follow the intensity profile of the target image, row by row. Each light thread is composed of a superposition of Bessel beams with equal separation in their longitudinal wavenumber, k_z—a superposition that can be physically realized using axicons with slightly different cone angles, as illustrated in Fig. 2b. Weighted by different complex coefficients, these co-propagating modes interfere along the optical path to construct any

 https://doi.org/10.1038/s41566-023-01188-y

arbitrary longitudinal intensity profile given by the function $F(z)$, as depicted in Fig. 2c. This approach is not limited to free-space propagation but can also be extended to cases in which the propagation medium is characterized by a complex refractive index (Supplementary Note 3). The underlying mechanism of this axial intensity modulation relies on the interplay between the energy in the centre spot of the beam and its outer rings. For example, when the central spot 'switches off', its energy is dispersed to the outer rings of the beam, albeit with less intensity, thus conserving the global energy at each cross-section (as shown in the bottom insets of Fig. 2c). The mathematical formulation of the surface frozen wave theory and the calculation of the complex weights of each Bessel mode in the superposition can be found in Methods. Note that previous work on surface frozen waves was only theoretical, studying simple patterns such as curved lines without considering the specifications of the display (for example, its resolution and pixel pitch). In the following, we provide an experimental demonstration of 2D and 3D holographic light sheets and examine their feasibility using commercially available LCD panels, as well as their advantages compared with multi-plane Fresnel holography.

Experimental generation

We generated our holographic sheets using programmable phase-only spatial light modulators (SLMs). We started by specifying the target image, the number of light threads (that is, frozen waves) over which the image would be discretized, the diameter of the light threads and the separation between them. In most of our examples, we discretized our target images into roughly 80 frozen waves, each with a centre spot radius of 30 µm separated by a 45 µm gap. Different combinations of these values will ultimately define the resolution of the projected image and are practically limited by the implementation medium, as detailed more fully in Supplementary Note 2. We calculated the superposition of Bessel beams comprising each frozen wave, then added all of the frozen waves spatially offset with respect to each other by a displacement of 45 µm, centre to centre. By solving for this superposition at the $z = 0$ plane, we obtained the complex transverse profile of the hologram in the x–y plane; this is the initial field distribution that would propagate in space to eventually construct the target image in the x–z plane. As our SLM can modulate the phase of an incident wavefront without altering its amplitude (as is the case for most holographic media), we deployed a phase retrieval algorithm to convert our complex (amplitude and phase) field distribution into a phase-only mask, following the method outlined in ref. 63 and Supplementary Note 5. This phase mask was then displayed on the SLM. In our experiment, we used a phase-only reflective SLM (Santec SLM-200) with a resolution of 1,920 × 1,200 pixels and 8 µm pixel pitch. The former parameter defines the aperture size of our hologram, which dictates the longitudinal extent of the projected image, and the latter sets an upper limit on the highest spatial frequency of the initial field distribution, which determines the largest cone angle for the Bessel modes in the superposition. The choice of these parameters and the implications are discussed more fully in Supplementary Note 2. As is standard in digital holography[63], the desired complex profile was generated at the output focal plane of a 4f imaging system located after the SLM (f being the focal length of the imaging lenses). The role of the 4f system is twofold: (1) to filter the desired pattern from the zeroth-order beam and (2) to image the filtered pattern onto the charge-coupled device (CCD). Note that we encoded our desired hologram off-axis by adding a blazed grating profile to the CGH to spatially separate it from the unmodulated zeroth-order beam (which arises due to the finite filling factor of the SLM). Figure 2d depicts the experimental set-up described above, where the $z = 0$ plane lies at the output focal plane of the 4f system. To construct the longitudinal profile of our light sheets, we recorded the transverse profile of the output pattern at each z plane with a CCD then stitched one-dimensional (1D) slices from those images together

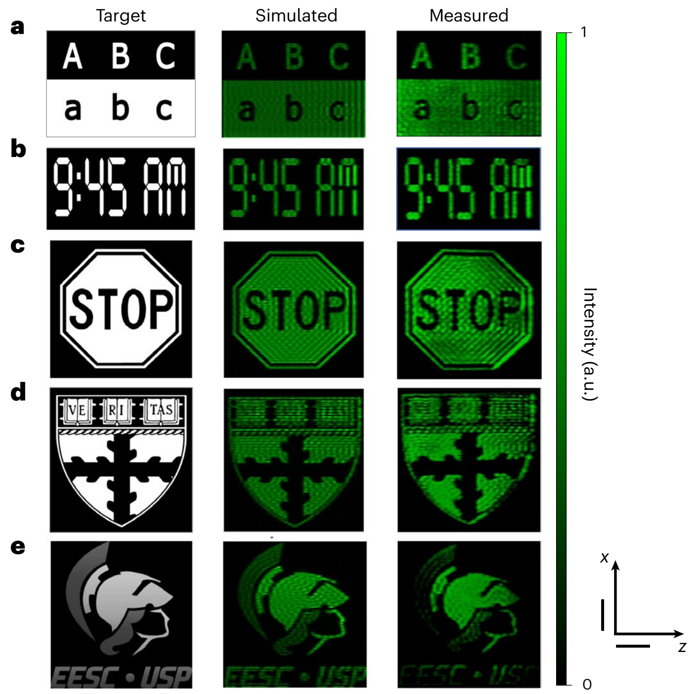

Fig. 3 | Generation of 2D holographic light sheets. a–**e**, The target image (left), simulated profile (middle) and reconstructed hologram (right) for three letters with dark and bright backgrounds (**a**), an alphanumerical pattern that mimics a digital alarm clock (**b**), a traffic sign (**c**), the Harvard University logo (**d**) and the University of São Paulo logo in multi-level greyscale (**e**). All images are projected in the horizontal (x–z) plane perpendicular to the SLM. The horizontal and vertical scale bars represent 10 mm and 0.5 mm (for simulations) and 2.5 mm and 0.125 mm (for measurements), respectively.

(via post processing) to reconstruct the image in the x–z plane. In the following, we demonstrate different examples of light sheets created by this approach and then show how the method could be extended to reconstruct 3D objects.

Results

We designed and generated several light sheet patterns projected along the direction of propagation. We start by demonstrating 2D patterns, and then generalize our method to create volumetric objects. All of our holograms were designed at the visible wavelength (532 nm) and were projected over a longitudinal range of 55 cm, but could easily be realized at other wavelengths and dimensions. Figure 3 exhibits five different profiles that have been holographically projected in the x–z plane, propagating from left to right in the plane normal to the SLM. In the first example (Fig. 3a), we projected three letters on dark and bright backgrounds to test the contrast of the output image. Both the dark background (top) and foreground (bottom), and the sharp boundary in between, were successfully reconstructed with high fidelity and contrast and without considerable interference between the forward-propagating light threads. Likewise, the round curvature and steep corners of the letters are all well defined. Similarly, in Fig. 3b, the dark background region of the digital clock was effectively realized with almost no residual contributions from the bright components of the image. Note how the smaller features of the image, namely the two dots of the colon, are intact and are in very good agreement with the target and simulated patterns. In Fig. 3c we show an example of a 'STOP' sign in which the sharp edges and narrow dark lines were all reconstructed with high resolution across the entire extent of the image. Holograms of this kind can potentially be deployed as dynamic traffic signs in public streets or garages.

https://doi.org/10.1038/s41566-023-01188-y

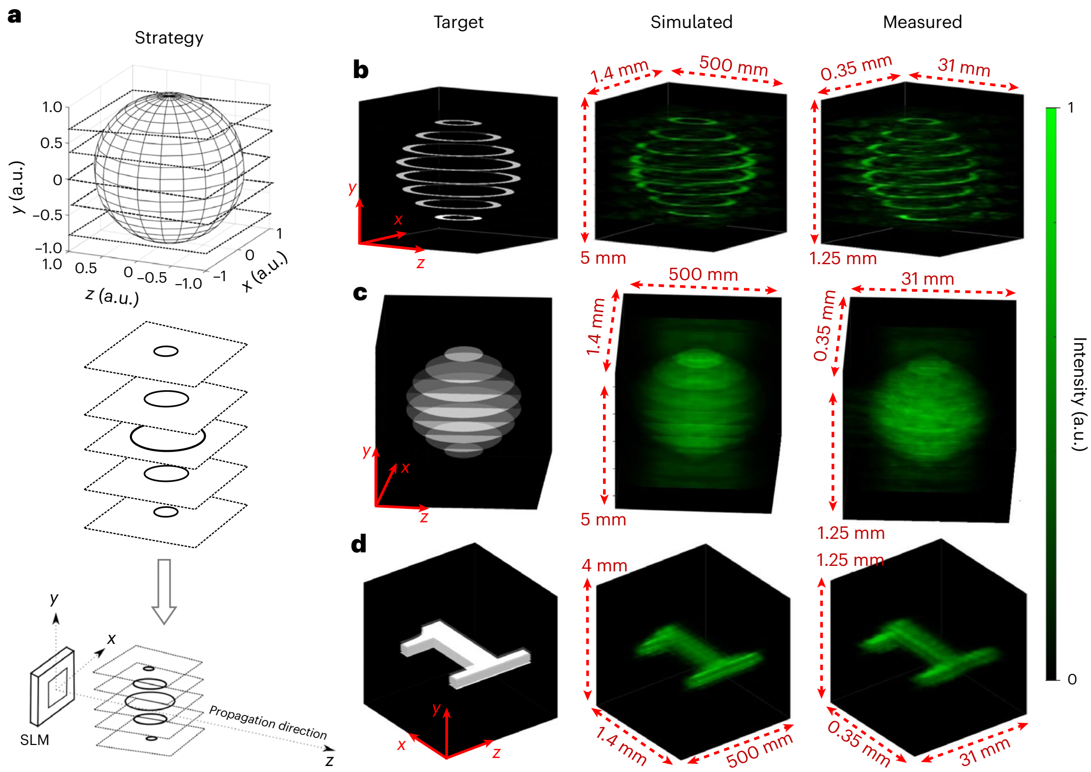

Fig. 4 | Assembling 2D holographic light sheets to construct volumetric (3D) scenes. a, The strategy relies on discretizing the target scene into 2D slices with small gaps between them. Each slice is decomposed into a number of co-propagating parallel light threads, for which the initial field distribution is calculated. The $z = 0$ field distributions for all 2D light sheets are all added then transformed into a single CGH, displayed onto an SLM. The SLM then projects the 2D stacks to create the desired 3D scene. **b**, The target (left) and simulated (middle) and experimental (right) reconstructions of a 3D sphere made of hollow rings (**b**), a 3D solid sphere (**c**) and a volumetric digit (**d**).

We also considered more complicated patterns, such as the logo of Harvard John A Paulson School of Engineering depicted in Fig. 3d. Although larger features such as the dark cross and overall print of the logo have been nicely constructed, resolving finer features (such as the 'VERITAS' motto) remains challenging. A quick comparison between the measured and simulated images reveals that it is not possible to fully resolve these letters even in theory with the current design parameters. However, this limitation is not fundamental, but stems from our choice of a parameter space that can be practically implemented using a commercial SLM (with pixel pitch $\delta x = 8$ μm). In practice, the pixel pitch limits the highest spatial frequency of the Bessel modes that can forward propagate such that $\max(k_\rho) \leq 1/\delta x$ (where k_ρ is the transverse component of the wavevector). Akin to a Fourier series in which a periodic function can be reconstructed by including higher-order sinusoidal terms in the superposition, the quality of each light thread—that is, each row of the projected image—depends on the total number of co-propagating Bessel beams and their spatial frequencies. In essence, an implementation medium that can offer smaller pixel pitch would allow Bessel modes with larger spatial frequencies to be included in the Bessel superposition, thus resolving all of these fine features. Metasurfaces[17,18,64] are perhaps among the most common platforms that can address this limitation given their subwavelength pixel pitch, which can easily enable the reconstruction of these holograms with at least 10× the current resolution. Alternatively, one could keep the spatial frequencies the same but use a larger display to project the logo over larger area where those tiny features can be resolved. In Supplementary Note 3 we relax some of these technical constraints and show simulation results of holograms with enhanced quality. The reconstructed images also exhibit weak intensity modulation (ripples) in regions where the intensity is supposed to be uniform. This stems from the underlying superposition of co-propagating Bessel beams in a manner that resembles a (truncated) Fourier series. Smoother intensity profiles are readily obtained by including more Bessel terms with higher spatial frequencies—a capability that can again be afforded with metasurfaces.

Importantly, while all four examples discussed so far have considered two-level (binary) intensity images, our approach can be applied to realize target images with multi-level intensity. This is demonstrated in Fig. 3e, in which we generate the logo of University of São Paulo's School of Electrical Engineering. In this case, some features (such as the helmet) have darker/brighter intensity levels than other regions of the image, yet are still constructed with high accuracy. Intensity gradients of this kind are often considered as critical cues for accurate depth perception.

These are only a few of the possibilities that could be realized with our holographic light sheets. It is important to note that we were able to fully control the projected image at the $y = 0$ plane and its vicinity (a sheet thickness of 60 μm), but had limited control over the intensity profile outside that region. This suggests that accurate construction of our holograms might (in some cases) be realized at the expense of undesired residual energy outside the plane of interest. In Supplementary Fig. 11 we examine these effects further by presenting additional 2D cuts of the constructed pattern outside the x–z plane. Unlike multi-plane Fresnel holography, however, this residue does not require non-uniform stacking of the 2D sheets when constructing a 3D volume (Supplementary Note 4).

Multi-chromatic light sheets

Thus far we have projected monochromatic 2D images along the optical path. Nevertheless, by superimposing three light sheets, representing the RGB channels, it is possible to generate a full colour image. This can potentially be implemented with a holographic medium that can impart three independent phase profiles on the blue, green and red wavelengths, simultaneously—a capability that has been realized efficiently with dispersion-engineered metasurfaces[64,65]. We provide a proof-of-concept demonstration for multi-chromatic sheets in Supplementary Fig. 13.

Projecting 3D objects

A stack of 2D holographic light sheets, oriented along the optical path, can be adequately cascaded to form a volumetric object. Figure 4a illustrates this concept: a target scene is decomposed into parallel planar slices with equal separation between them. Each 2D slice is composed of forward-propagating light threads for which the initial field distribution (at the $z = 0$ plane) could be analytically obtained, as discussed before. The initial field distributions associated with each 2D slice are then superimposed and transformed into a single CGH that can be displayed on an SLM following the procedure used in ref. 63 and detailed in Supplementary Note 5. When illuminated by a quasi-plane wave, the SLM will project all 2D slices, in parallel, thus constructing the target volume.

To illustrate our strategy, we designed and measured a number of 3D holograms. For example, in Fig. 4b we show a sphere composed of eight hollow rings, each separated by a gap of 0.477 mm. The designed pattern extends for 50 cm in the z direction and occupies roughly 0.5 cm in the transverse direction. It is worth noting that the sphere is relatively stretched along the longitudinal direction. This stems from our choice to operate in the paraxial regime (setting the longitudinal length of the target image L to 55 cm), which mandates the use of Bessel beams with small cone angles. Nevertheless, the aspect ratio can be adjusted by tuning the parameters of the hologram or by changing the magnification ratio of the 4f lens system after the SLM. In our experiments we used a demagnification ratio of 4:1. This scales down the projected hologram by 1/4× and 1/16× in the transverse and longitudinal directions, respectively, as explained in Supplementary Note 2. The measured pattern thus exhibited a more realistic aspect ratio and its spatial profile was in good agreement with simulation, demonstrating the ability of our approach to resolve each ring despite the close interspacing. Similarly, in Fig. 4c, we show a projected solid sphere composed of eight bright circles, separated by 0.468 mm, realizing a true 3D volume with continuous depth sampling (reconstruction) along the z direction, uniform sampling in the transverse direction and with very high contrast of approximately −20 dB.

Our method can also be applied to create volumetric dark regions, which often arise due to phase singularities in the optical field[66]. Owing to their steep phase gradients, singular light fields can exhibit interesting super-oscillatory behaviour and have thus been utilized in metrology. In Supplementary Fig. 14 we show an example where we created a dark hollow sphere in a background of brightness—a light structure that can be exploited in 3D sensing or cloaking applications. In Fig. 4d we also reduced the spacing between the slices to about 100 μm to project a volumetric digit '1', which is displayed with minimum background noise. Crosstalk between different layers can be reduced by increasing the separation between the image planes (albeit at the expense of larger display) or by deploying tricks from signal processing (for example, adding random phase noise as demonstrated in ref. 35 or using machine learning-based optimization). These potential improvements and others will be the subject of future work.

Discussion

In this work we introduced light sheet holography, a new class of hologram that can project the target image along the direction of light propagation. Unlike Fourier and Fresnel-based holography, which discretize a 3D scene along the optical path, inevitably affecting the axial resolution and depth perception, our approach allows the desired scene to be reconstructed continuously in the axial direction with uniform discretization in the lateral direction. The axial resolution of our proposed scheme is ultimately limited by the pixel pitch of the implementation medium and could achieve tenfold the reported values by deploying metasurfaces for wavefront control at the subwavelength scale.

Our longitudinally oriented holographic light sheets could be favourable in applications that mandate high axial resolution and continuous depth for true-to-life depth perception, and in configurations where the hologram is preferably viewed from the side to avoid direct transmission towards the viewer, reducing eye fatigue. Note that the finite resolution of SLMs, our platform of choice, inevitably sets a constraint on the viewing angle. However, this limitation (commonly referred to as the space–bandpath product) can be mitigated using clever arrangements of optics around the display to provide the necessary momentum kick[59,67]. Importantly, due to their resistance to attenuation and self-healing characteristics (Supplementary Note 3), our light sheets could be utilized as part of a volumetric display by projecting multi-layered light sheets onto a stack of diffusive or frosted glass plates or through a suspension of micro-scatterers to directly view the whole real 3D images simultaneously[58,59]. In Supplementary Videos 1–3 we illustrate how our holograms can, in principle, be viewed over the full 4π solid angle if used in volumetric displays.

In summary, we provide a systematic approach that enables the projection of any 2D image or 3D scene onto light sheets with high fidelity and contrast. A quantitative analysis of the reconstruction quality compared with traditional Fresnel holography can be found in Extended Data Figs. 1 and 2 and in Supplementary Note 4, suggesting reduced inter-plane crosstalk using our approach. Our design strategy is based on non-iterative analytic closed-form expressions with calculable computation time. As our holograms are composed of forward-propagating Bessel modes, they can be scaled to any dimensions and wavelengths by following the same design considerations as axicons[61]. In Supplementary Note 2 we show how the dimensions of our holographic light sheets can be scaled in size, both digitally (by tuning the parameters of the CGH) and optically (by changing the 4f lens configuration after the SLM). While this work was focused on scalar light sheets with the same polarization state, it is possible to incorporate Bessel modes of different polarizations to create 3D scenes with spatially varying polarization[68]. In this regard, one could also weave the 2D sheet from light threads of alternating orthogonal polarizations to minimize the interference between adjacent light threads, as illustrated in Supplementary Note 3. Finally, besides using programmable SLMs, dynamic control of our holographic sheets can readily be achieved using active metasurfaces[69], or using OAM metasurface holography in which real-time switching between the holographic scenes is enabled by changing the spatial structure of the incident beam[70]. We thus expect this new class of hologram to inspire new uses in wearable devices, volumetric displays, light sheet microscopy and other emerging applications.

Online content

Any methods, additional references, Nature Portfolio reporting summaries, source data, extended data, supplementary information, acknowledgements, peer review information; details of author contributions and competing interests; and statements of data and code availability are available at https://doi.org/10.1038/s41566-023-01188-y.

References

1. Sheridan, J. T. et al. Roadmap on holography. *J. Optics* **22**, 123002 (2020).
2. Gabor, D. A new microscopic principle. *Nature* **161**, 777–778 (1948).
3. Blanche, P.-A. et al. Holographic three-dimensional telepresence using large-area photorefractive polymer. *Nature* **468**, 80–83 (2010).

4. Heanue, J. F., Bashaw, M. C. & Hesselink, L. Volume holographic storage and retrieval of digital data. *Science* **265**, 749–752 (1994).
5. Pégard, N. C. & Fleischer, J. W. Optimizing holographic data storage using a fractional Fourier transform. *Opt. Lett.* **36**, 2551–2553 (2011).
6. Schilling, B. W. et al. Three-dimensional holographic fluorescence microscopy. *Opt. Lett.* **22**, 1506–1508 (1997).
7. Kim, M. K. *Digital Holographic Microscopy* 149–190 (Springer, 2011).
8. Dickey, F. M. *Laser Beam Shaping: Theory and Techniques* 2nd edn (CRC, 2014).
9. Padgett, M. & Bowman, R. Tweezers with a twist. *Nat. Photon.* **5**, 343–348 (2011).
10. Maimone, A., Georgiou, A. & Kollin, J. S. Holographic near-eye displays for virtual and augmented reality. *ACM Trans. Graph.* **36**, 1–16 (2017).
11. Kohler, C., Schwab, X. & Osten, W. Optimally tuned spatial light modulators for digital holography. *Appl. Opt.* **45**, 960–967 (2006).
12. Forbes, A., Dudley, A. & McLaren, M. Creation and detection of optical modes with spatial light modulators. *Adv. Opt. Photon.* **8**, 200–227 (2016).
13. Ren, Y.-X., Lu, R.-D. & Gong, L. Tailoring light with a digital micromirror device. *Ann. Phys.* **527**, 447–470 (2015).
14. Lee, B. et al. Wide-angle speckleless DMD holographic display using structured illumination with temporal multiplexing. *Opt. Lett.* **45**, 2148–2151 (2020).
15. Moerner, W. E., Grunnet-Jepsen, A. & Thompson, C. L. Photorefractive polymers. *Annu. Rev. Mater. Sci.* **27**, 585–623 (1997).
16. Malek, S. C., Ee, H.-S. & Agarwal, R. Strain multiplexed metasurface holograms on a stretchable substrate. *Nano Lett.* **17**, 3641–3645 (2017).
17. Genevet, P. & Capasso, F. Holographic optical metasurfaces: a review of current progress. *Rep. Progr. Phys.* **78**, 024401 (2015).
18. Huang, L., Zhang, S. & Zentgraf, T. Metasurface holography: from fundamentals to applications:. *Nanophotonics* **7**, 1169–1190 (2018).
19. Cutting, J. E. & Vishton, P. M. in *Perception of Space and Motion* (eds Epstein, W. & Rogers, S.) 69–117 (Academic, 1995).
20. Yatagai, T. Stereoscopic approach to 3-D display using computer-generated holograms. *Appl. Opt.* **15**, 2722–2729 (1976).
21. Tajahuerce, E. & Javidi, B. Encrypting three-dimensional information with digital holography. *Appl. Opt.* **39**, 6595–6601 (2000).
22. Dorsch, R. G., Lohmann, A. W. & Sinzinger, S. Fresnel ping-pong algorithm for two-plane computer-generated hologram display. *Appl. Opt.* **33**, 869–875 (1994).
23. Makowski, M., Sypek, M., Kolodziejczyk, A. & Mikula, G. Three-plane phase-only computer hologram generated with iterative Fresnel algorithm. *Opt. Eng.* **44**, 125805 (2005).
24. Mishina, T., Okui, M. & Okano, F. Calculation of holograms from elemental images captured by integral photography. *Appl. Opt.* **45**, 4026–4036 (2006).
25. Wakunami, K., Yamaguchi, M. & Javidi, B. High-resolution three-dimensional holographic display using dense ray sampling from integral imaging. *Opt. Lett.* **37**, 5103–5105 (2012).
26. Yamaguchi, M., Hoshino, H., Honda, T. & Ohyama, N. in *Practical Holography VII: Imaging and Materials* Vol. 1914 (ed. Benton, S. A.) 25–31 (SPIE, 1993).
27. Barabas, J., Jolly, S., Smalley, D. E. & Bove Jr, V. M. in *Practical Holography XXV: Materials and Applications* Vol. 7957 (ed. Bjelkhagen, H. I.) 13–19 (SPIE, 2011).
28. Zhang, H., Zhao, Y., Cao, L. & Jin, G. Fully computed holographic stereogram based algorithm for computer-generated holograms with accurate depth cues. *Opt. Express* **23**, 3901–3913 (2015).
29. Padmanaban, N., Peng, Y. & Wetzstein, G. Holographic near-eye displays based on overlap-add stereograms. *ACM Trans. Graph.* **38**, 1–13 (2019).
30. Chen, J.-S. & Chu, D. P. Improved layer-based method for rapid hologram generation and real-time interactive holographic display applications. *Opt. Express* **23**, 18143–18155 (2015).
31. Zhao, Y., Cao, L., Zhang, H., Kong, D. & Jin, G. Accurate calculation of computer-generated holograms using angular-spectrum layer-oriented method. *Opt. Express* **23**, 25440–25449 (2015).
32. Zhang, J., Pégard, N., Zhong, J., Adesnik, H. & Waller, L. 3D computer-generated holography by non-convex optimization. *Optica* **4**, 1306–1313 (2017).
33. Wei, Q., Huang, L., Li, X., Liu, J. & Wang, Y. Broadband multiplane holography based on plasmonic metasurface. *Adv. Opt. Mater.* **5**, 1700434 (2017).
34. Piao, M.-L. et al. Multi-depth three-dimensional image encryption based on the phase retrieval algorithm in the Fresnel and fractional Fourier transform domains. *Appl. Opt.* **57**, 7609–7617 (2018).
35. Makey, G. et al. Breaking crosstalk limits to dynamic holography using orthogonality of high-dimensional random vectors. *Nat. Photon.* **13**, 251–256 (2019).
36. Zhou, Y. et al. Multifunctional metaoptics based on bilayer metasurfaces. *Light Sci. Appl.* **8**, 80 (2019).
37. Zheng, G., Fu, R., Deng, L., Li, G. & Li, Z. On-axis three-dimensional meta-holography enabled with continuous-amplitude modulation of light. *Opt. Express* **29**, 6147–6157 (2021).
38. Tay, S. et al. An updatable holographic three-dimensional display. *Nature* **451**, 694–698 (2008).
39. Smalley, D. E. et al. A photophoretic-trap volumetric display. *Nature* **553**, 486–490 (2018).
40. Hernandez, O. et al. Three-dimensional spatiotemporal focusing of holographic patterns. *Nat. Commun.* **7**, 11928 (2016).
41. Almeida, E., Bitton, O. & Prior, Y. Nonlinear metamaterials for holography. *Nat. Commun.* **7**, 12533 (2016).
42. Huang, L. et al. Three-dimensional optical holography using a plasmonic metasurface. *Nat. Commun.* **4**, 2808 (2013).
43. Yu, H., Lee, K., Park, J. & Park, Y. Ultrahigh-definition dynamic 3D holographic display by active control of volume speckle fields. *Nat. Photon.* **11**, 186–192 (2017).
44. Makowski, P. L., Kozacki, T., Zdankowski, P. & Zaperty, W. Synthetic aperture Fourier holography for wide-angle holographic display of real scenes. *Appl. Opt.* **54**, 3658–3665 (2015).
45. Lucente, M. E. Interactive computation of holograms using a look-up table. *J. Electron. Imaging* **2**, 28–34 (1993).
46. Kim, S.-C. & Kim, E.-S. Fast computation of hologram patterns of a 3D object using run-length encoding and novel look-up table methods. *Appl. Opt.* **48**, 1030–1041 (2009).
47. Chen, R. H.-Y. & Wilkinson, T. D. Computer generated hologram with geometric occlusion using GPU-accelerated depth buffer rasterization for three-dimensional display. *Appl. Opt.* **48**, 4246–4255 (2009).
48. Ren, H., Shao, W., Li, Y., Salim, F. & Gu, M. Three-dimensional vectorial holography based on machine learning inverse design. *Sci. Adv.* **6**, eaaz4261 (2020).
49. Shi, L., Li, B., Kim, C., Kellnhofer, P. & Matusik, W. Towards real-time photorealistic 3D holography with deep neural networks. *Nature* **591**, 234–239 (2021).
50. Lesem, L. B., Hirsch, P. M. & Jordan, J. A. The kinoform: a new wavefront reconstruction device. *IBM J. Res. Dev.* **13**, 150–155 (1969).

51. Lee, W. H. Sampled Fourier transform hologram generated by computer. *Appl. Opt.* **9**, 639–643 (1970).
52. Haddad, W. S. et al. Fourier-transform holographic microscope. *Appl. Opt.* **31**, 4973–4978 (1992).
53. Alexandrov, S. A., Hillman, T. R., Gutzler, T. & Sampson, D. D. Synthetic aperture Fourier holographic optical microscopy. *Phys. Rev. Lett.* **97**, 168102 (2006).
54. Zheng, G., Horstmeyer, R. & Yang, C. Wide-field, high-resolution Fourier ptychographic microscopy. *Nat. Photon.* **7**, 739–745 (2013).
55. Plesniak, W., Pappu, R., Underkoffler, J., Lucente, M. & St.-Hilaire, P. in *Holographic Imaging* (eds Benton, S. A. & Bove, V. M.) Ch. 19 (Wiley, 2008).
56. Gülses, A. A. & Jenkins, B. K. Cascaded diffractive optical elements for improved multiplane image reconstruction. *Appl. Opt.* **52**, 3608–3616 (2013).
57. Jackin, B. J. & Yatagai, T. 360° reconstruction of a 3D object using cylindrical computer generated holography. *Appl. Opt.* **50**, H147–H152 (2011).
58. Huebschman, M. L., Munjuluri, B. & Garner, H. R. Dynamic holographic 3-D image projection. *Opt. Express* **11**, 437–445 (2003).
59. Zabels, R., Osmanis, K., Narels, M., Smukulis, R. & Osmanis, I. in *Advances in Display Technologies IX* Vol. 10942 (eds Lee, J.-H. et al.) 51–61 (SPIE, 2019).
60. Zamboni-Rached, M. Stationary optical wave fields with arbitrary longitudinal shape by superposing equal frequency Bessel beams: frozen waves. *Opt. Express* **12**, 4001–4006 (2004).
61. McGloin, D. & Dholakia, K. Bessel beams: diffraction in a new light. *Contemp. Phys.* **46**, 15–28 (2005).
62. Ambrosio, L. A. Millimeter-structured nondiffracting surface beams. *J. Opt. Soc. Am. B* **36**, 638–645 (2019).
63. Arrizón, V., Ruiz, U., Carrada, R. & González, L. A. Pixelated phase computer holograms for the accurate encoding of scalar complex fields. *J. Opt. Soc. Am. A* **24**, 3500–3507 (2007).
64. Dorrah, A. H. & Capasso, F. Tunable structured light with flat optics. *Science* **376**, eabi6860 (2022).
65. Chen, W. T., Zhu, A. Y. & Capasso, F. Flat optics with dispersion-engineered metasurfaces. *Nat. Rev. Mater.* **5**, 604–620 (2020).
66. Lim, S. W. D., Park, J.-S., Meretska, M. L., Dorrah, A. H. & Capasso, F. Engineering phase and polarization singularity sheets. *Nat. Commun.* **12**, 4190 (2021).
67. Park, J., Lee, K. & Park, Y. Ultrathin wide-angle large-area digital 3D holographic display using a non-periodic photon sieve. *Nat. Commun.* **10**, 1304 (2019).
68. Dorrah, A. H., Rubin, N. A., Zaidi, A., Tamagnone, M. & Capasso, F. Metasurface optics for on-demand polarization transformations along the optical path. *Nat. Photon.* **15**, 287–296 (2021).
69. Shaltout, A. M., Shalaev, V. M. & Brongersma, M. L. Spatiotemporal light control with active metasurfaces. *Science* **364**, eaat3100 (2019).
70. Ren, H. et al. Metasurface orbital angular momentum holography. *Nat. Commun.* **10**, 2986 (2019).

Methods

Formulation of holographic light sheets

The fabric of our holograms is a 2D light sheet composed of an array of light threads. A pictorial visualization of a 2D light sheet (or a surface frozen wave) and its decomposition into light threads is shown in Supplementary Fig. 3. Each thread, formally known as a frozen wave[60], is composed of a discrete superposition of co-propagating zeroth-order Bessel beams with different wavevectors. Owing to the constructive and destructive interference among these co-propagating modes, the intensity of the resulting waveform would be modulated with propagation in space. The choice of Bessel beams as the co-propagating modes is not fundamental, but advantageous: first, they possess self-healing and non-diffracting properties that keep the central spot of the beam intact over a long distance even in the presence of obstruction[61]; and second, being an exact solution to the wave equation, they allow a complete analytical description of the field. An array of P frozen waves (where P is the number of frozen waves) can construct a surface frozen wave[62] that in cylindrical coordinates can be represented as the Fourier series:

$$\psi(\rho,\phi,z,t) = \mathrm{e}^{-i\omega t}\sum_{q=1}^{P}\sum_{m_q=-N}^{N} A^{(m_q)} J_0\left(k_\rho^{(m_q)}\sqrt{\rho^2+\rho_{0q}-2\rho\rho_{0q}\cos(\phi-\phi_{0q})}\right)\mathrm{e}^{ik_z^{(m_q)}z}. \tag{1}$$

The J_0 term denotes a zeroth-order Bessel mode propagating along the z direction, whereas $k_\rho^{(m_q)}$ and $k_z^{(m_q)}$ are the transverse and longitudinal wavevectors, respectively, $(k_\rho^{(m_q)})^2+(k_z^{(m_q)})^2=(\omega/c)^2$. In addition, m_q is the index of each Bessel beam in the superposition, ω is the angular frequency and t is time. Each individual frozen wave is positioned at (ρ_{0q},ϕ_{0q}), and its Bessel mode components are each weighted by a different complex coefficient $A^{(m_q)}$. The longitudinal wavevectors are chosen according to their corresponding Bessel mode:

$$k_z^{(m_q)} = \mathbf{Q}+\frac{2\pi m_q}{L}, \tag{2}$$

where $\mathbf{Q}$ is the central longitudinal wavevector chosen on the basis of experimental parameters and L is the desired longitudinal length of the target image; that is, $z < L$.

The longitudinal intensity pattern of each and every light thread can be designed to follow any arbitrary profile—denoted as $F_q(z)$ —by properly selecting the complex coefficient through a Fourier integral:

$$A^{(m_q)} = \frac{1}{L}\int_0^L \mathbf{F}_q(z)\mathrm{e}^{-i\frac{2\pi}{L}m_q z}\,\mathrm{d}z, \tag{3}$$

Therefore, the intensity profile of the light sheet can be designed to represent any arbitrary 2D profile along the direction of propagation. The complex coefficients $A^{(m_q)}$ are substituted in equation (1) to evaluate ψ, which locally approximates the desired response, $\mathbf{F}_q(z)$. In essence, a wavefront-shaping medium that takes the form $\psi(\rho,\phi,z=0,t)$ at an initial z plane, transverse to the longitudinal direction, will be able to recreate the desired field distribution at each consecutive z plane thereafter to display the 2D field in the x–z plane. Note that because Bessel beams ideally contain an infinite number of outer rings (with infinite energy), we instead used Bessel–Gauss beams in equation (1) to generate our CGHs over a finite aperture. We discuss this in more detail in Supplementary Note 2.

Experimental set-up

Our measurements were obtained using a 532 nm laser source (Novanta Photonics, Ventus Solid State CW laser). The beam was expanded and collimated by focusing it with an objective lens (40×) through a 50 μm pinhole followed by a 50 cm lens. The collimated beam was directed onto a reflective SLM (Santec SLM-200, 1,920 × 1,200 pixel resolution and 8 μm pixel pitch), encoding the desired phase-only hologram onto the beam. A 4f lens system was placed after the SLM to filter the desired pattern in the k space from on-axis (zeroth-order) noise and to image the beam onto a CCD camera after demagnifying it by a factor of ×1/4. The CCD camera (Thorlabs DCU224C, 1,280 × 1,024 resolution) was mounted on an automated translational z stage (Thorlabs LTS150) to record the 2D and 3D holographic images along the propagation direction. The transverse profiles were recorded at each z plane with increments of 0.25 mm along the propagation direction. From each recorded image, a 1D slice (at the location of the light sheet) was extracted; these 1D slices were in turn concatenated in the longitudinal direction to reconstruct the final 2D and 3D holographic scenes. The contrast in our holograms was obtained from the CCD intensity measurements I, and is defined as $10\log_{10}\frac{I_{\min}}{I_{\max}}$.

Data availability

All key data that support the findings of this study are included in the article and its Supplementary Information. Additional datasets and raw measurements are available from the corresponding authors upon reasonable request.

Code availability

The codes and simulation files that support Figs. 1–4, Extended Data Figs. 1 and 2 and the data analysis are available from the corresponding authors upon reasonable request.

Acknowledgements

We thank A. Zaidi, A. Palmieri and M. Greiner, all of Harvard University, as well as M. Ritsche-Marte of the Medical University of Innsbruck for insightful discussions. A.H.D. acknowledges financial support from the Natural Sciences and Engineering Research Council of Canada (NSERC) under award no. PDF-533013-2019. F.C. acknowledges financial support from the Office of Naval Research (ONR) under the MURI programme, grant no. N00014-20-1-2450, and from the Air Force Office of Scientific Research (AFOSR) under grant nos FA9550-21-1-0312 and FA9550-22-1-0243. V.S.d.A. acknowledges financial support from the National Council for Scientific and Technological Development (CNPq) under grant no. 140270/2022-1. M.Z.-R. acknowledges financial support from CNPq under grant no. 306689/2019-7 and from São Paulo Research Foundation (FAPESP) under grant no 2021/15027-8. L.A.A. acknowledges financial support from CNPq under grant no. 309201/2021-7 and from FAPESP under grant nos 2020/05280-5 and 2021/06121-0.

Author contributions

A.H.D. designed and built the experiment, created the CGHs with input from P.B. and analysed and processed the data. P.B. performed the measurements and acquired and processed the data. V.S.d.A. and J.O.d.S developed the MATLAB simulations of surface frozen waves. M.Z.-R. conceived the frozen wave theory. L.A.A. developed the mathematical formulation of surface frozen waves. F.C. supervised the project. A.H.D., P.B. and F.C. wrote the paper with input from all co-authors.

Competing interests

The authors have filed a provisional patent application based on this work.

Additional information

Extended data is available for this paper at https://doi.org/10.1038/s41566-023-01188-y.

https://doi.org/10.1038/s41566-023-01188-y

Supplementary information The online version contains supplementary material available at https://doi.org/10.1038/s41566-023-01188-y.

Correspondence and requests for materials should be addressed to Ahmed H. Dorrah or Federico Capasso.

Peer review information *Nature Photonics* thanks Fatih Ilday, YongKeun Park and the other, anonymous, reviewer(s) for their contribution to the peer review of this work.

https://doi.org/10.1038/s41566-023-01188-y

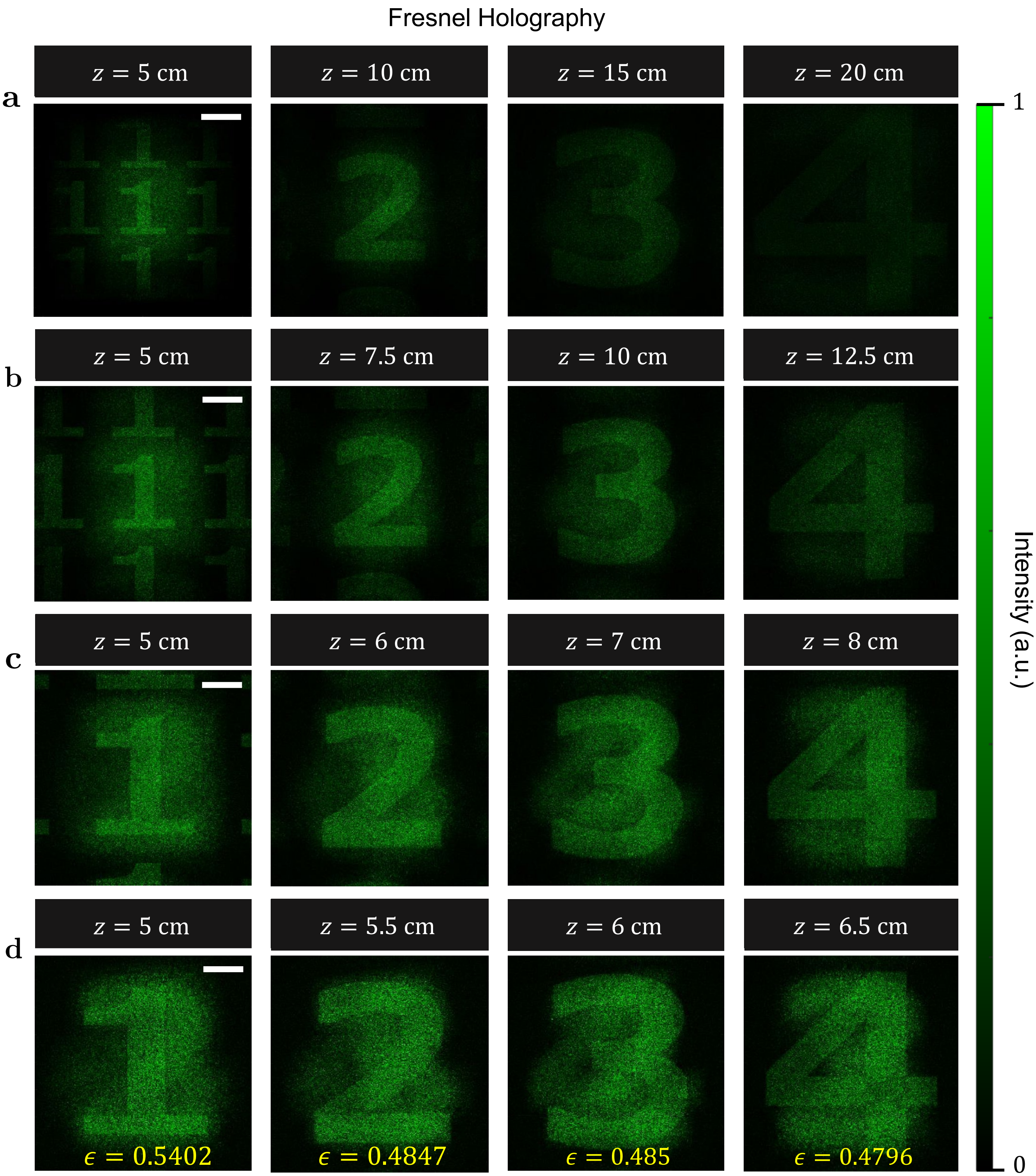

Extended Data Fig. 1 | See next page for caption.

https://doi.org/10.1038/s41566-023-01188-y

Extended Data Fig. 1 | Projecting 2D images with Fresnel holography. Four digits '1 2 3 4' are axially projected along the propagation direction. The longitudinal separation between the image planes is (a) 5 cm, (b) 2.5 cm, (c) 1 cm, and (d) 0.5 cm. The scale bars in (a-d) are 2 mm, 1.5 mm, 1 mm and 0.8 mm, respectively. While cross-talk can be reduced by placing the images further apart (a), the size of the displayed images vary significantly (becoming larger) at longer propagation distances. This magnification can be mitigated by reducing the separation between the images, however, at the expense of more significant cross-talk (d). Here, ϵ depicts the reconstruction error as detailed in Supplementary Note 4.

 https://doi.org/10.1038/s41566-023-01188-y

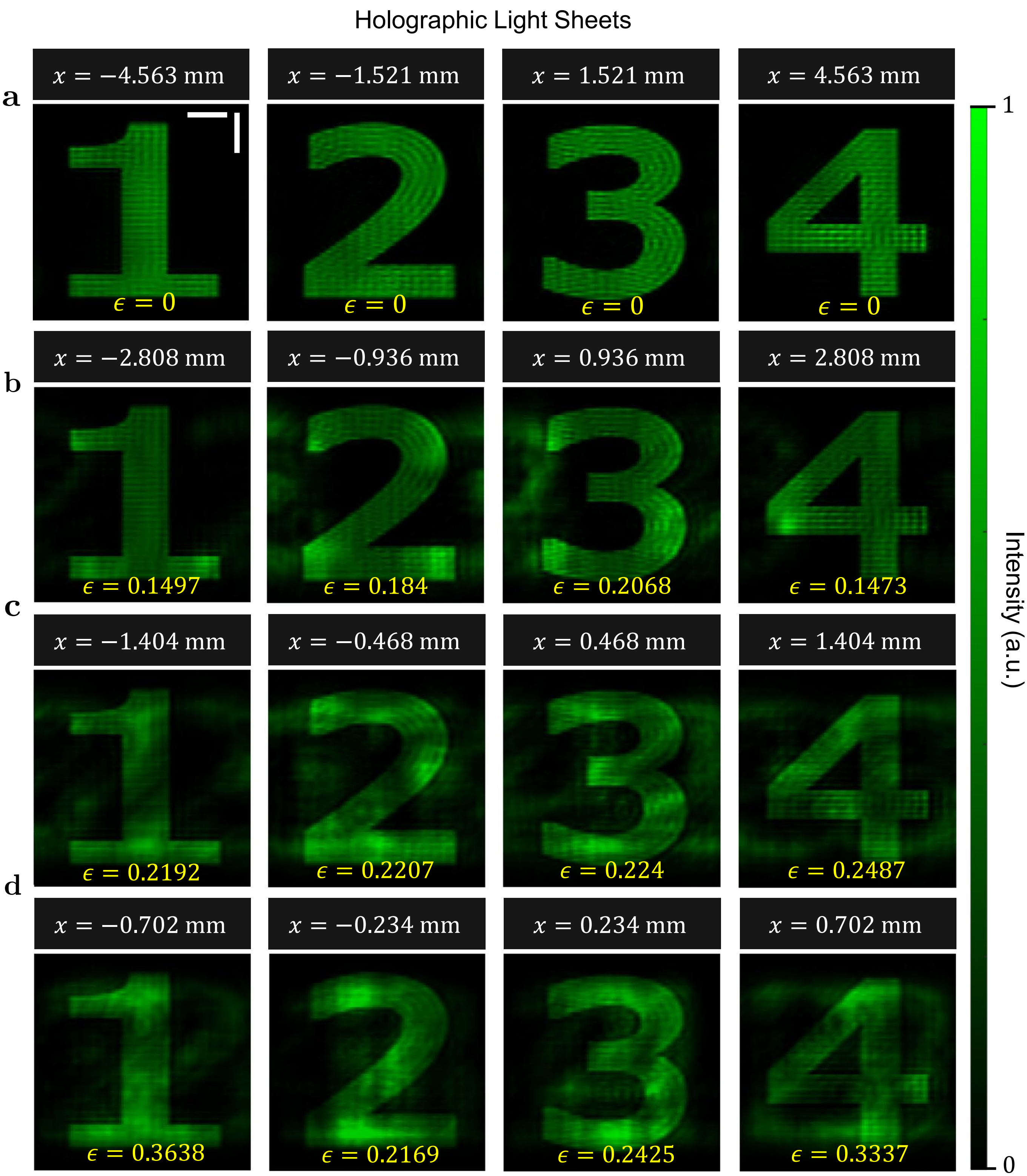

Extended Data Fig. 2 | Projecting 2D images with holographic light sheets. Four digits '1 2 3 4' are projected in the lateral direction perpendicular to the display. The lateral separation between the images is (a) 3.042 mm, (b) 1.872 mm, (c) 0.936 mm, and (d) 0.468 mm. The horizontal and vertical scale bars are 10 mm and 0.5 mm, respectively. Here, cross-talk (signified by ϵ) can be reduced by placing the images further apart in the lateral direction without affecting the size of the projected images. Furthermore, given their non-diffracting behavior, our holographic light sheets exhibit a relatively smooth profile (with less grainy features) compared to Fresnel-based multi-plane techniques.